The Astrophysical Journal, 648:1020–1025, 2006 September 10

A TESTABLE STOCHASTIC ACCELERATION MODEL FOR FLARES IN SAGITTARIUS A*

Siming Liu,[1] Vahé Petrosian,[2] Fulvio Melia,[3] and Christopher L. Fryer[1,4]

Received 2006 March 6; accepted 2006 May 25

ABSTRACT

The near-IR and X-ray flares in Sagittarius A* are believed to be produced by relativistic electrons via synchrotron and synchrotron self-Comptonization, respectively. These electrons are likely energized by turbulent plasma waves through second-order Fermi acceleration that, in combination with the radiative cooling processes, produces a relativistic Maxwellian distribution in the steady state. This model has four principal parameters, namely the magnetic field B, the electron density n and temperature $\gamma_c m_e c^2$, and the size of the flare region R. In the context of stochastic acceleration, the quantities $Rn^{1/2}B$ and $\gamma_c Rn$ should remain nearly constant in time. Therefore, simultaneous spectroscopic observations in the NIR and X-ray bands can readily test the model, which, if proven to be valid, may be used to determine the evolution of the plasma properties during an eruptive event with spectroscopic observations in either band or simultaneous flux density measurements in both bands. The formulae can be applied to other isolated or confined systems, where electrons are accelerated to relativistic energies by plasma wave turbulence and produce most of the emission via synchrotron processes.

Subject headings: acceleration of particles — black hole physics — Galaxy: center — plasmas — radiation mechanisms: thermal — turbulence

Online material: color figures

1. INTRODUCTION

Sagittarius A*, the compact radio source at the Galactic center, is powered by accretion onto an $M \sim (3-4) \times 10^6\ M_\odot$ supermassive black hole (Schödel et al. 2002; Ghez et al. 2004; Melia 2006). There is compelling evidence that the near-IR (NIR) flares in Sagittarius A* are produced by relativistic electrons via synchrotron emission within a few Schwarzschild radii of the black hole [Genzel et al. 2003; the Schwarzschild radius $r_S = 10^{12}(M/3.4 \times 10^6\ M_\odot)$ cm]. Inverse Compton scattering of the NIR photons by the same electrons produces X- and γ-ray emission, which may account for the observed X-ray flares (Baganoff et al. 2001, 2003; Goldwurm et al. 2003; Porquet et al. 2003; Bélanger et al. 2006). Simultaneous multiwavelength observations during a handful of flares have generally supported this hypothesis (Eckart et al. 2004, 2006; Bélanger et al. 2005; Yusef-Zadeh et al. 2006). However, our knowledge of the flare energization and electron acceleration mechanisms is still very rudimentary, although some details are starting to emerge (Liu et al. 2004, 2006; Tagger & Melia 2006; Bromley et al. 2001; Broderick & Loeb 2005).

The first NIR spectroscopic observations at a frequency $\nu \simeq 1.4 \times 10^{14}$ Hz revealed very soft power spectra, $\nu F_\nu \propto \nu^\alpha$, with index $-4 < \alpha < -2$ (Eisenhauer et al. 2005), indicating a sharp cutoff in the electron distribution. Such a cutoff is a natural consequence of stochastic acceleration (SA) by plasma waves, in which low-energy electrons are accelerated up to a relativistic energy, where radiative cooling becomes important (Schlickeiser 1984; Park & Petrosian 1995). In Sagittarius A*, the X-ray flare luminosity is always lower than that of the NIR events, so synchrotron cooling dominates. More recent NIR observations also indicate that F_ν may be correlated with α (Ghez et al. 2005; Gillessen et al. 2006; S. Hornstein et al. 2006, in preparation).

Flares in Sagittarius A* are likely driven by an accretion instability (e.g., Tagger & Melia 2006), which triggers the transfer of gravitational energy of the plasma into turbulence. In earlier work, we demonstrated that if thermal synchrotron and synchrotron self-Comptonization are the dominant emission mechanisms during Sagittarius A*'s flares, simultaneous X-ray and NIR spectroscopic observations (SSOs) can measure the size of the flare region R, the electron density n and "temperature" $\gamma_c m_e c^2$, and the magnetic field B (Liu et al. 2006). Interestingly, most of the flares are found to be local events with source size $R < r_S$, which can also explain the quasi-periodic modulations observed in some flares (see also Liu et al. 2004). This justifies the neglect of the source structure as a zero-order approximation and suggests that the flares involve highly dynamical activity and that the electron acceleration process has to be addressed to uncover the underlying physical processes.

In this paper, we consider steady state electron populations produced via SA by turbulent plasma waves, which, in combination with the synchrotron cooling, results in a relativistic Maxwellian distribution. The electron temperature is set by the energy diffusion and synchrotron cooling rates. The latter depends only on B, while the former is given by a combination of B, n, and R, which together imply that the product $\gamma_c nR$ should not vary significantly as the flare evolves, nor from one flare to the next. Moreover, since electrons gain energy from the plasma waves, overall energy conservation requires that the luminosity be equal to the energy transfer rate from turbulence, which also depends only on B, n, and R. This requires $Bn^{1/2}R$ to be constant. These two system constraints effectively reduce the model parameters to just two, so that SSOs can readily test the model.

Previous work on the flares is summarized in § 2, where we discuss differences between these models and assess the merit of previous proposed scenarios on the definiteness of their predictions and/or whether the model parameters can be well constrained by observations. The electron acceleration is described

[1] Los Alamos National Laboratory, Los Alamos, NM 87545; liusm@lanl.gov.
[2] Center for Space Science and Astrophysics, Department of Physics and Applied Physics, Stanford University, Stanford, CA 94305; vahe@astronomy.stanford.edu.
[3] Physics Department and Steward Observatory, University of Arizona, Tucson, AZ 85721; melia@physics.arizona.edu; Sir Thomas Lyle Fellow and Miegunyah Fellow.
[4] Physics Department, University of Arizona, Tucson, AZ 85721; fryer@lanl.gov.

in § 3. And in § 4 the model is applied to an NIR flare with a very hard spectrum. The model predictions and its limitations are discussed in § 5.

2. PREVIOUS WORK

Several models have been proposed since the *Chandra* discovery of a bright X-ray flare from Sagittarius A* (Baganoff et al. 2001; Markoff et al. 2001; Liu & Melia 2002; Yuan et al. 2004; Nayakshin et al. 2004). The facts that the flare variation timescale is comparable to the orbital period at the last stable orbit and that there is a good correlation between the X-ray and the strongly polarized NIR emission suggest that the flares are produced very close to the black hole. The nature of the correlation between an X-ray flare and a delayed radio outburst, on the other hand, indicates that the radio emission may be produced at large radii (Zhao et al. 2004). In the jet model studied by Markoff et al. (2001), it was assumed that the electrons and protons are Maxwellian and have the same temperature, and that the plasma near the base of the jet, which is within a few Schwarzschild radii of the black hole, is heated suddenly to a higher temperature during flares via shocks or magnetic field reconnection. By changing the physical conditions at the base of the jet, they were able to reproduce the observed X-ray flux. The distinct spectral and polarization characteristics of submillimeter emission, on the other hand, suggests that this radiation is produced by a small hot magnetized accretion torus near the black hole (Melia et al. 2000, 2001). The flat spectrum of the X-ray flares then motivated us to consider the production of X-rays via bremsstrahlung during an accretion instability (Liu & Melia 2002). To reduce the model parameters, the electrons and protons were assumed in thermal equilibrium in this calculation. Yuan et al. (2004) later considered a more complicated accretion model, in which the electrons and protons have different temperatures and there is a nonthermal component in the electron distribution prescribed by the choice of particle acceleration processes. With the temperature for the thermal component, the spectral index, high-energy cutoff, and normalization factor characterizing the nonthermal component as free parameters, it can accommodate a variety of flare spectra.

All these models are still consistent with the limited NIR and X-ray observations, due in part to the large number of model parameters and the relative paucity of data. It is clear that one must address the electron acceleration mechanism in order to (possibly) distinguish between these various models. Given the physical conditions in the emission region—those of a hot, magnetized plasma—it is natural to suppose that the electrons are being accelerated by plasma waves (e.g., Dermer et al. 1996), whose turbulent energy is fed from an accretion-induced instability. However, given the uncertainties in the generation of turbulence, and in the cascade and damping processes, several parameters were introduced to describe the turbulence spectrum (Liu et al. 2004). Not surprisingly, as was the case for the previous models, the available observations could not provide rigorous constraints on the parameters. Nevertheless, this first attempt at building a physical model suggested that some of the flares are actually produced within a region smaller than the size of the black hole, indicating that they are likely events localized in certain portions of the disk.

The discovery of NIR flares with very soft spectra implies a sharp cutoff in the relativistic electron distribution producing the polarized NIR emission via synchrotron. For typical conditions near the black hole inferred from the modeling of Sagittarius A*'s quiescent emission (Melia et al. 2001; Yuan et al. 2003), the synchrotron cooling time of electrons producing NIR emission is also comparable to the flare variation timescale and may therefore be the cause of the cutoff. Subsequent work with this model showed that the electron acceleration may be insensitive to the details of the turbulence spectrum and that such a cutoff is a natural consequence of SA of electrons by turbulence (Liu et al. 2006). Moreover, if the injection of particles into the acceleration region is slow, the electron spectrum in steady state may be approximated as a relativistic Maxwellian distribution. In this case, there are only four model parameters, namely the source size R, the electron temperature $\gamma_c m_e c^2$ and density n, and the magnetic field B. This model has therefore now matured to the point at which its parameters may be readily determined by SSOs. Of course, this does not yet mean that SA is solely responsible for accelerating the electrons. Other mechanisms may also produce similar distributions.

3. SA OF ELECTRONS BY PLASMA WAVES

Tagger & Melia (2006) first showed that the Rossby wave instability in a small accretion torus can reproduce the characteristics of the flare light curves. In such a picture the gravitational energy of protons and ions is released by this macroscopic instability, which generates the turbulence on a scale comparable to R. The turbulence then cascades toward small scales and accelerates electrons in the process. It is clear that the whole plasma in the turbulent region can be energized by the gravitational energy release. We therefore do not need a continuous injection of electrons at low energies. Moreover, since the plasma is gravitationally trapped by the black hole, the accelerated electrons will not escape from the acceleration region as long as their energy is lower than the gravitational binding energy of the protons, which is comparable to the protons rest mass energy. The evolution of an electron distribution $N(\gamma,\ t)$ under the influence of a turbulent magnetic field is given therefore by (Blandford & Eichler 1987)

$$\frac{\partial N}{\partial t} = \frac{\partial}{\partial \gamma}\left(\frac{\gamma^4}{\tau_{\rm ac}}\frac{\partial \gamma^{-2} N}{\partial \gamma} + \frac{\gamma^2}{\tau_0} N\right), \tag{1}$$

where $\gamma = 100\gamma_2$ is the Lorentz factor[5] and the synchrotron cooling and acceleration times are given, respectively, by

$$\tau_{\rm syn}(\gamma) = \frac{\tau_0}{\gamma} \equiv \frac{9 m_e^3 c^5}{4 e^4 B^2 \gamma} = 21.56 B_1^{-2}\gamma_2^{-1}\ {\rm hr}, \tag{2}$$

$$\tau_{\rm ac} \equiv \frac{2\gamma^2}{\langle \Delta\gamma \Delta\gamma/\Delta t\rangle} = \frac{C_1 3Rc}{v_{\rm A}^2} = 52.49 C_1 R_{12} n_7 B_1^{-2}\ {\rm hr}, \tag{3}$$

where $v_{\rm A} = B/(4\pi n m_p)^{1/2} = 6.901\times 10^8 B_1 n_7^{-1/2}$ cm s^{-1} is the Alfvén velocity, $B_1 = B/10$ G, $n_7 = n/10^7$ cm^{-3}, $R_{12} = R/10^{12}$ cm, and C_1 is a dimensionless quantity that depends on the microscopic details of the wave-particle interaction and is of order 1 if the scattering mean-free path is comparable to R, which may be smaller than the Schwarzschild radius ($\sim 10^{12}$ cm) of the black hole. The other constants have their usual meaning. Note that in equation (3) the velocity of the scatterers in the original SA proposed by Fermi (1949) has been replaced by the Alfvén velocity $v_{\rm A}$. This may not be always true, especially when the sound velocity $v_s > v_{\rm A}$. The exact dependence of $\tau_{\rm ac}$ on v_s and $v_{\rm A}$ is still under investigation. Because v_s also depends on the proton temperature, which is an input in the model, here we focus on the simplest scenario, where the effects of sound waves are ignored. And as we see below, particle-particle collisions can be

[5] Here we have assumed that the direct acceleration rate $\langle \Delta\gamma/\Delta t\rangle/\gamma$ is equal to the energy diffusion rate $\langle \Delta\gamma\Delta\gamma/\Delta t\rangle'/\gamma$, as is usually true in SA by plasma waves, where a prime indicates a derivative with respect to γ. In a more general case, where the direct acceleration rate $\langle \Delta\gamma/\Delta t\rangle/\gamma = p\langle \Delta\gamma\Delta\gamma/\Delta t\rangle'/\gamma$ the first term on the right-hand side of eq. (1) should be $[\gamma^{4p}\tau_{\rm ac}^{-1}(\gamma^{2-4p}N)']'$.

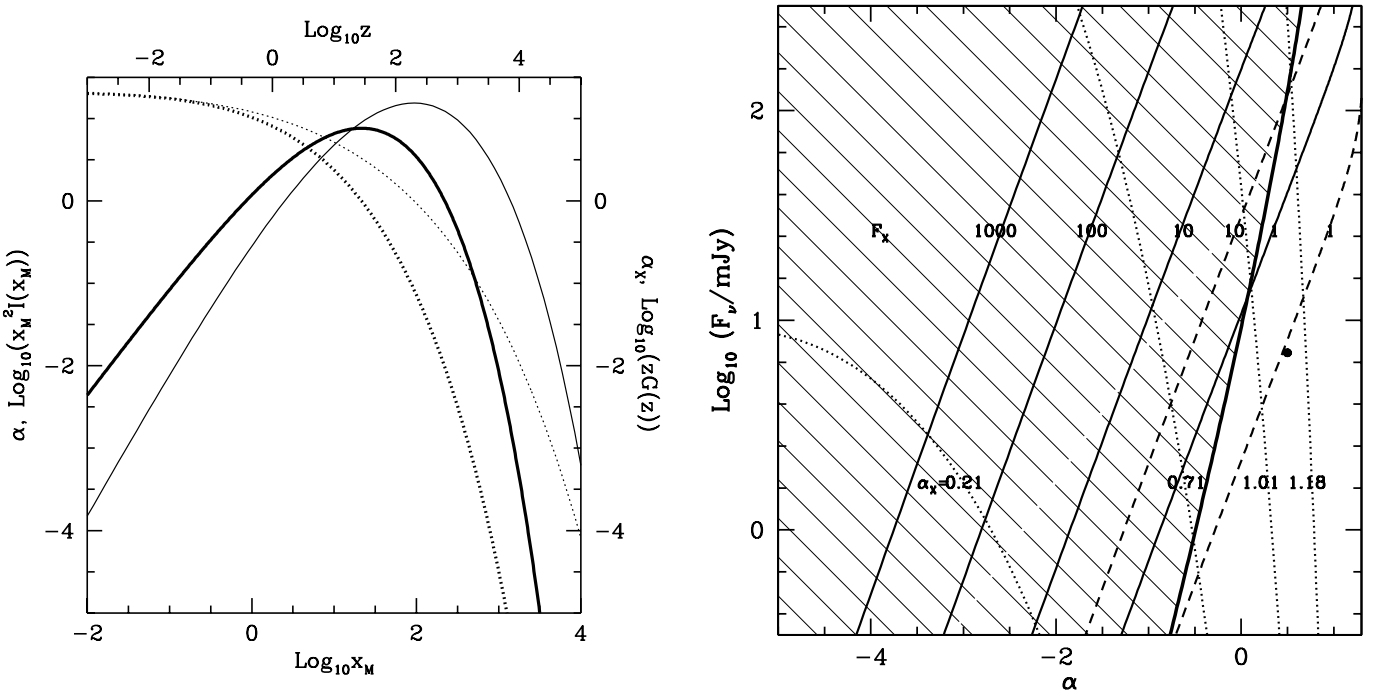

FIG. 1.—*Left:* Thermal synchrotron (*thick lines*) and self-Comptonization (*thin lines*) power spectral index (*dotted line*) and normalized energy flux density νF_ν (*solid line*) as functions of their normalized frequencies. *Right*: Correlation between the NIR ($\nu_{14} = 1.429$) and X-ray ($\nu_{18} = 1.0$) spectral indexes and flux densities for $C_1 = C_2 = D_8 = 1.0$. The horizontal and vertical axes are for the NIR spectral index and flux density, respectively. The dotted and solid lines indicate constant X-ray spectral index and flux density (in units of the quiescent level of 0.015 μJy) with the corresponding value labeled on the lines. The dashed lines are similar to the solid lines but with $C_1 = 0.5$. The filled circle indicates the model studied in the paper. The steady state solution may not be valid in the shaded region. See text for details. [*See the electronic edition of the Journal for a color version of this figure*.]

ignored, and the electrons are mainly scattered by the turbulence. Since the inferred particle pressure is much higher than the magnetic field pressure, R is the only length scale in the system and should be comparable to the particle mean-free-path. If the flares are triggered by instabilities that are similar from event to event, C_1 should be nearly constant. In steady state this yields[6]

$$N(\gamma) = \frac{n\gamma^2}{2\gamma_c^3}\exp\left(\frac{-\gamma}{\gamma_c}\right), \quad \text{with } \gamma_c = \frac{\tau_0}{\tau_{\rm ac}} = 41.08 C_1^{-1} R_{12}^{-1} n_7^{-1}. \tag{4}$$

The normalization of N is accurate to order γ_c^{-2}. Therefore $\gamma_c Rn$ only depends on the instabilities and should not change significantly with time.

4. RELATIVISTIC MAXWELLIAN SYNCHROTRON EMISSION AND SELF-COMPTONIZATION

The thermal synchrotron flux density and emission coefficient (i.e., emissivity divided by the solid angle) are given, respectively, by (Petrosian 1981; Mahadevan et al. 1996)

$$F_\nu = \frac{4\pi R^3}{3D^2}\mathcal{E}_\nu, \qquad \mathcal{E}_\nu = \frac{\sqrt{3}e^3}{8\pi m_e c^2} Bn x_M I(x_M), \tag{5}$$

where

$$I(x_M) = 4.0505 x_M^{-1/6}\left(1 + 0.40 x_M^{-1/4} + 0.5316 x_M^{-1/2}\right) \times \exp\left(-1.8899 x_M^{1/3}\right), \tag{6}$$

$$x_M = \nu/\nu_c \equiv 4\pi m_e c\nu/3eB\gamma_c^2 = 1412 C_1^2 \nu_{14} R_{12}^2 n_7^2 B_1^{-1}, \tag{7}$$

[6] For the more general case mentioned above, $N(\gamma) \propto \gamma^{4p-2}\exp(-\gamma/\gamma_c)$.

$\nu = \nu_{14} 10^{14}$ Hz, and the distance to the Galactic center $D = D_8 8$ kpc. The spectral index in a given narrow frequency range is therefore

$$\alpha \equiv \frac{d\ln(\nu F_\nu)}{d\ln\nu} = 1.833 - 0.6300 x_M^{1/3} - \frac{0.1000 x_M^{1/4} + 0.2658}{x_M^{1/2} + 0.4000 x_M^{1/4} + 0.5316}, \tag{8}$$

and the flux density may be written

$$F_\nu = \frac{e^3}{2\sqrt{3}m_e c^2}\frac{BnR^3}{D^2} x_M I(x_M) = 639.7 R_{12}^3 n_7 B_1 D_8^{-2} x_M I(x_M)\ \text{mJy}. \tag{9}$$

The thick lines in Figure 1 (*left*) show this spectral index (*dotted line*) and the normalized spectrum $x_M^2 I(x_M)$ (*solid line*), as functions of the normalized frequency x_M.

We can estimate the energy transfer rate in a fully developed turbulence from dimensional analysis:

$$\mathcal{L}_{\rm Turb} = C_2 v_{\rm A} B^2 R^2 = 6.901 \times 10^{34} C_2 R_{12}^2 n_7^{-1/2} B_1^3 \ \text{ergs s}^{-1}, \tag{10}$$

where C_2 is another dimensionless quantity that only depends on the turbulence generation mechanism and therefore remains nearly a constant.[7] If there are no other significant energy loss

[7] Here $\mathcal{L}_{\rm Turb}$ could be a complicated function of v_s and $v_{\rm A}$. We, however, focus on the simplest case.

processes, this energy transfer rate should be equal to the source luminosity ($\mathcal{L} \simeq \mathcal{L}_{\rm syn}$) in the steady state, where

$$\mathcal{L}_{\rm syn} = \left(64\pi e^4/9m_e^2c^3\right)nR^3B^2\gamma_c^2 = 8.949\times10^{34}C_1^{-2}R_{12}n_7^{-1}B_1^2 \text{ ergs s}^{-1}. \quad (11)$$

We therefore infer that

$$R_{12}n_7^{1/2}B_1 = 1.297C_1^{-2}C_2^{-1}, \quad (12)$$

a condition that should not change significantly with time either. We note that the electron advection occurs on the accretion time, which can be more than 10 times longer than the dynamical time. This term is negligible during flares (see § 5). And even though there are other energy loss processes, such as the diffusive escape of accelerated particles and/or the propagation of waves away from the flare region (Petrosian & Liu 2004), we expect that an approximately fixed fraction of the released energy goes into radiation. This constraint is still valid.

For given values of C_1 and C_2, spectroscopic observations in the NIR band then can be used to determine the properties of the flaring plasma. First from equation (8) and the observed spectral index α, one can obtain x_M, which in combination with equations (7) and (6) and the observed frequency gives ν_c and $I(x_M)$. Then one can use the measured flux density and equations (7), (9), and (12) to obtain R, n, and B, and γ_c can be inferred with equation (4). For the bright NIR flare observed by Ghez et al. (2005), $\alpha = 0.5$, $\nu_{14} = 1.429$, and $F_\nu = 7$ mJy, we have $x_M = 7.314$, $x_M I(x_M) = 0.7811$, $\nu_c = 1.954\times10^{13}(x_M/7.314)^{-1}(\nu_{14}/1.429)$ Hz,

$$R_{12} = 0.08471C_1^2C_2^{6/7}D_8^{10/7}\left(\frac{x_M}{7.314}\right)^{-1/7}\left[\frac{x_MI(x_M)}{0.7811}\right]^{-5/7}\times\left(\frac{\nu_{14}}{1.429}\right)^{1/7}\left(\frac{F_\nu}{7\text{ mJy}}\right)^{5/7}, \quad (13)$$

$$n_7 = 2.266C_1^{-4}C_2^{-10/7}D_8^{-12/7}\left(\frac{x_M}{7.314}\right)^{4/7}\left[\frac{x_MI(x_M)}{0.7811}\right]^{6/7}\times\left(\frac{\nu_{14}}{1.429}\right)^{-4/7}\left(\frac{F_\nu}{7\text{ mJy}}\right)^{-6/7}, \quad (14)$$

$$B_1 = 10.17C_1^{-2}C_2^{-8/7}D_8^{-4/7}\left(\frac{x_M}{7.314}\right)^{-1/7}\left[\frac{x_MI(x_M)}{0.7811}\right]^{2/7}\times\left(\frac{\nu_{14}}{1.429}\right)^{1/7}\left(\frac{F_\nu}{7\text{ mJy}}\right)^{-2/7}, \quad (15)$$

$$\gamma_c = 214.0C_1C_2^{4/7}D_8^{2/7}\left(\frac{x_M}{7.314}\right)^{-3/7}\left[\frac{x_MI(x_M)}{0.7811}\right]^{-1/7}\times\left(\frac{\nu_{14}}{1.429}\right)^{3/7}\left(\frac{F_\nu}{7\text{ mJy}}\right)^{1/7}. \quad (16)$$

All these values are consistent with the results of previous studies (Liu et al. 2004, 2006). The electron-electron collision time, $\tau_c = \gamma m_e^2c^3/8\pi ne^4\ln\Lambda \simeq 1164\gamma_2n_7^{-1}$ hr ($\ln\Lambda = 40$ in this case) is much longer than any other timescale. Particle-particle collisions, therefore, may be ignored. The electron pressure ($\sim n\gamma_c m_e c^2$) is about 5 times higher than the magnetic field pressure. The total particle pressure could be much higher.

From Kirchhoff's law, the synchrotron absorption coefficient

$$\kappa_\nu = \mathcal{E}_\nu/2\gamma_c m_e\nu^2 = \left(\pi en/3\sqrt{3}\gamma_c^5B\right)[I(x_M)/x_M],$$

and we have the optical depth through the emission region

$$\tau_\nu \equiv \kappa_\nu R = 2.482C_1^5R_{12}^6n_7^6B_1^{-1}[I(x_M)/x_M] = 1.783\times10^{-7}C_1^{-5}C_2^{-16/7}D_8^{-8/7}\left(\frac{x_M}{7.314}\right)^{-2}\left[\frac{x_MI(x_M)}{0.7811}\right], \quad (17)$$

so the source is optically thin above $x_M = 1.766\times10^{-3}$, i.e., for ν exceeding 34.52 GHz. Then the photon energy density

$$U \simeq \frac{\mathcal{L}_{\rm syn}}{4\pi cR^2} = 127.9C_1^{-4}C_2^{-12/7}D_8^{-6/7}\left(\frac{x_M}{7.314}\right)^{-5/7}\left[\frac{x_MI(x_M)}{0.7811}\right]^{3/7}\times\left(\frac{\nu_{14}}{1.429}\right)^{5/7}\left(\frac{F_\nu}{7\text{ mJy}}\right)^{-3/7}\text{ ergs cm}^{-3} \quad (18)$$

is more than 3 times lower than that of the magnetic field, justifying our neglect of the self-Comptonization cooling[8]

The self-Comptonization flux density is then given by (Blumenthal & Gould 1970)

$$F_{\rm X}(\nu) \simeq \frac{2\pi e^7n^2BR^4}{3\sqrt{3}m_e^3c^6D^2}G\left(\frac{\nu}{4\nu_c\gamma_c^2}\right) = 2.121n_7^2B_1R_{12}^4D_8^{-2}G\left(\frac{\nu}{4\nu_c\gamma_c^2}\right)\ \mu\text{Jy}, \quad (19)$$

where

$$G(z) = z\int_0^\infty dx\times\int_0^1 dy\ \exp(-x)I\left(zx^{-2}y^{-1}\right)\left(2\ln y + 1 - 2y + y^{-1}\right), \quad (20)$$

the low limit of the integral over $x = \gamma/\gamma_c$ has been extended from $1/\gamma_c$ to 0, which simplifies the formula and introduces a less than 0.2% error, and $z = \nu/4\nu_c\gamma_c^2$.

Similarly, one can define the spectral index

$$\alpha_{\rm X} \equiv d\ln(\nu F_{\rm X})/d\ln\nu = 1 + d\ln G(z)/d\ln z. \quad (21)$$

The normalized power spectrum $zG(z)$ and $\alpha_{\rm X}$ are depicted by thin lines in Figure 1 (*left*).

For the above mentioned NIR flare, the model predicts that in the *Chandra* and *XMM-Newton* bands ($\nu^{\rm X} = \nu_{18}^{\rm X}10^{18}$ Hz, which corresponds to ~4.2 keV)

$$z = 0.28C_1^{-2}C_2^{-8/7}D_8^{-4/7}\nu_{18}^{\rm X}\left(\frac{x_M}{7.314}\right)^{13/7}\left[\frac{x_MI(x_M)}{0.7811}\right]^{2/7}\times\left(\frac{\nu_{14}}{1.429}\right)^{-13/7}\left(\frac{F_\nu}{7\text{ mJy}}\right)^{-2/7}, \quad (22)$$

$$\alpha_{\rm X}(z) = 1.1, \quad (23)$$

$$F_{\rm X}(z) = 0.0033C_1^{-2}C_2^{-4/7}D_8^{-2/7}\left[\frac{G(z)}{0.58}\right]\left(\frac{x_M}{7.314}\right)^{3/7}\times\left[\frac{x_MI(x_M)}{0.7811}\right]^{-6/7}\left(\frac{\nu_{14}}{1.429}\right)^{-3/7}\left(\frac{F_\nu}{7\text{ mJy}}\right)^{6/7}\ \mu\text{Jy}, \quad (24)$$

[8] The self-Comptonization effects may be incorporated into the model by replacing the B^2 with $B^2 + 8\pi U$ in the electron cooling and source luminosity terms.

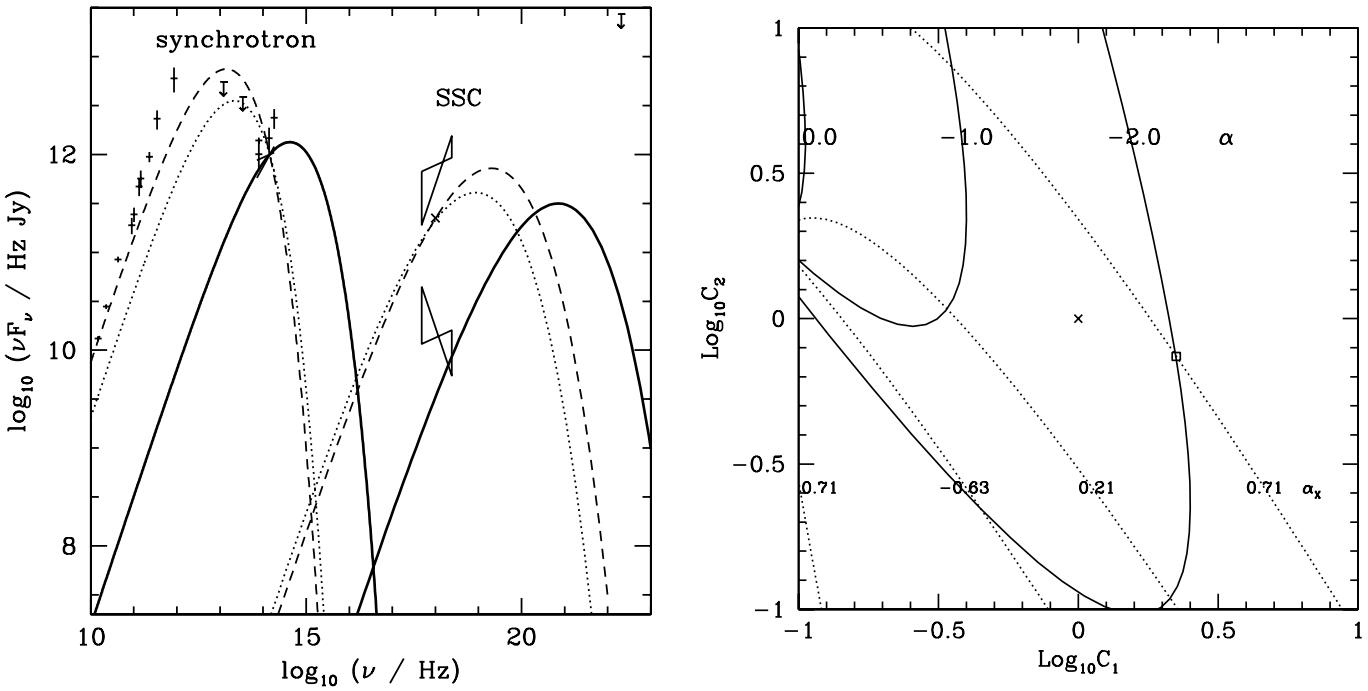

FIG. 2.—*Left:* Model fit to the NIR flare studied in the paper (*solid line*) and the peak flux densities of the brightest flare observed simultaneously in the NIR and X-ray bands by Eckart et al. (2006). For the latter, $F_\nu = 7$ mJy and $F_X = 0.223$ μJy. $C_1 = C_2 = 1.0$ for the dotted line, and $C_1 = 2.2$, $C_2 = 0.74$ for the dashed line. Note that the effect of self-absorption is not included here. The right panel shows the dependence of the model predicted NIR (α) and X-ray (α_X) spectral indexes on C_1 and C_2 for this flare. We expect a soft NIR spectrum with $\alpha < 0.0$ for reasonable values of C_1 and C_2. [*See the electronic edition of the Journal for a color version of this figure.*]

which is about 5 times below the quiescent flux level. We therefore do not expect a detectable X-ray flux accompanying this flare. From equations (22) and (24), one obtains the correlation between the NIR and X-ray spectroscopic observations. For a given X-ray spectral index, which is a function of z, equation (22) gives the dependence of the NIR flux density on x_M, which determines α. For a given X-ray flux density F_X, one obtains x_M as a function of z by eliminating the F_ν terms in the two equations. This gives F_ν as a function of α with x_M as a parametric variable. These two relations are plotted in Figure 1 (*right*) for $C_1 = C_2 = D_8 = 1.0$. Here F_X is in units of Sagittarius A*'s quiescent flux density of 0.015 μJy at 4.2 keV.

5. DISCUSSION AND CONCLUSIONS

First, we notice that for weak NIR flares with very hard spectra (to the bottom right of the right-hand panel of Fig. 1), there is little X-ray emission and that X-ray flares are expected to accompany NIR flares with soft spectra (to the left). These predictions may be readily tested via a statistical study of all the observed flare events (Hornstein et al. 2002) and explain why the occurrence rate of NIR flares is more than two times greater than that of the X-ray events. For NIR flares with very hard spectra, α_X is also large (corresponding to a hard spectrum), we expect hard X-ray/γ-ray emission, especially during bright NIR flares (to the top-right).

Second, brighter X-ray flares (to the top left) tend to have higher NIR fluxes and softer NIR spectra. The spectral index α_X is also small to the left. We expect little γ-ray emission accompanying weak NIR flares with very soft spectra (to the bottom-left).

Third, for a given α, F_X is roughly proportional to F_ν. The spectral index α_X correlates with F_ν for low values of α, but this correlation almost vanishes for positive α. For low values of α, we also expect a correlation between F_X and α_X.

Finally, the results are very sensitive to the values of C_1 and C_2. The dashed lines in the figure indicates X-ray flares with $C_1 = 0.5$. These are quite different from the lines with $C_1 = 1.0$. For the referenced NIR flare, the X-ray flux will be detectable with *Chandra* for $C_1 = 0.5$. Thus, C_1 and C_2 may be determined accurately with SSOs.

Some of these predictions are shown explicitly in the left panel of Figure 2, where the solid lines are the model spectra of the synchrotron and self-Comptonization components for the NIR flare studied above. Although there is little X-ray emission, we expect γ-ray emission up to a few MeV during the flare. The model is also applied to the brightest flare observed simultaneously in the NIR and X-ray bands by Eckart et al. (2004) during their multiwavelength campaign in 2004. The NIR and X-ray fluxes correlated well during the flare and the peak flux densities $F_\nu = 7$ mJy and $F_X = 0.223$ μJy. The spectral indexes of the flare have not been published yet. Because the X-ray flux is high, we expect soft NIR spectra. The dotted (with $C_1 = C_2 = 1.0$) and dashed (with $C_1 = 2.2$, $C_2 = 0.74$) lines are for this flare. The right panel shows how the NIR and X-ray spectral indexes depend on C_1 and C_2. The cross and square correspond to the dotted and dashed lines in the left panel, respectively. These show that for given flux densities the spectral indexes are very sensitive to the values of C_1 and C_2. Because both C_1 and C_2 are dimensionless quantities, we expect them to be on the order of 1. The model therefore predicts that the NIR emission has a soft spectrum with $\alpha < 0$.

For the referenced NIR flare the electron acceleration time

$$\tau_{\rm ac} = 5.845 C_1^3 C_2^{12/7} D_8^{6/7} \left(\frac{x_M}{7.314}\right)^{5/7} \left[\frac{x_M I(x_M)}{0.7811}\right]^{-3/7} \times \left(\frac{\nu_{14}}{1.429}\right)^{-5/7} \left(\frac{F_\nu}{7\ {\rm mJy}}\right)^{3/7} \ {\rm minutes} \quad (25)$$

is shorter than the dynamical time of $\tau_{\rm dy} \sim 20$ minutes, which is consistent with the observed flare variation time, justifying our usage of the steady state solution, which, however, may not be valid when $\tau_{\rm ac} > \tau_{\rm dy}$, as indicated by the shaded area in

Figure 1 (*right*). Note that for the NIR flares with softer spectra we studied before (Liu et al. 2006), $\alpha < -2.0$, the steady state solution therefore may not be applicable. In the most general cases, both τ_{ac} and τ_0 are functions of t, which are determined by the large-scale MHD processes. Time-dependent solutions of equation (1) $N(\gamma, t)$ are needed. However, we do not expect the electron distribution to be radically different from Maxwellian. By introducing a time-dependent $\gamma_c(t)$, the results here may be readily generalized to incorporate the time evolution of the system and applied to the accretion flow in the quiescent state when advection can be important. One may also have to take into account the Doppler and gravitational effects as the emitting plasma is likely moving on a Keplerian orbit near the black hole (Bromley et al. 2001; Broderick & Loeb 2005). These are beyond the scope of the current investigation.

Since the discovery of NIR and X-ray flares in Sagittarius A*, several models have been proposed (Markoff et al. 2001; Liu & Melia 2002). Given the uncertainties in the electron acceleration mechanism, earlier models prescribe either the electron distribution (Yuan et al. 2004) or the turbulence spectrum (Liu et al. 2004) with several free parameters resulting in all kinds of emission spectra. In previous work (Liu et al. 2006), we showed that Sagittarius A*'s flare activity might be explained with thermal synchrotron and self-Comptonization emission, and all the model parameters, namely, B, n, R, and γ_c, could be readily determined by SSOs. In this paper we have shown that the electrons are likely heated by turbulence, which produces a Maxwellian distribution and predicts two time-insensitive constraints on the plasma properties making the model testable with SSOs. This is the first model that can be tested with current instrument capability. We have provided general expressions for the emission spectra and demonstrated how properties of the flaring plasma may be inferred from the spectroscopic observations or simultaneous flux measurements in both bands.

The model may therefore provide powerful tools for studying physical processes near the event horizon of black holes. A time-dependent treatment of this problem will make it possible to compare MHD simulations of the black hole accretion with the observed flare activity in Sagittarius A*, which will eventually lead to a measurement of the black hole's spin after the instability is identified and light propagation effects are incorporated properly. (Note that for the referenced NIR flare, the electron Lorentz factor $\gamma_c \sim 200$ already suggests that the gravitational energy release beyond the last stable orbit of a Schwarzschild black hole is not sufficient to power the flare.) The formulae for the thermal synchrotron and self-Comptonization emission are valid so long as optically thin synchrotron emission dominates the radiative output and may therefore be applicable to other astrophysical sources, particularly low-luminosity-AGNs.

We thank Mark Morris, Seth Hornstein, and Marco Fatuzzo for useful discussion. This work was funded in part under the auspices of the US Department of Energy and supported by its contract W-7405-ENG-36 to Los Alamos National Laboratory. This research was partially supported by NSF grant ATM 03-12344, NASA grants NAG5-12111, NAG5-11918-1 (at Stanford), NSF grant AST 04-02502 (at Arizona), and NSF grant PHY 99-07949 (at KITP at UCSB). F. M. is very grateful to the University of Melbourne for its support (through a Miegunyah Fellowship).

REFERENCES

Baganoff, F. K., et al. 2001, Nature, 413, 45
———. 2003, ApJ, 591, 891
Bélanger, G., Goldwurm, A., Melia, F., Ferrando, P., Grosso, N., Porquet, N., Warwick, R., & Yusef-Zadeh, F. 2005, ApJ, 635, 1095
Bélanger, G., et al. 2006, ApJL, submitted
Blandford, R., & Eichler, D. 1987, Phys. Rep., 154, 1
Blumenthal, G. R., & Gould, R. J. 1970, Rev. Mod. Phys., 42, 237
Broderick, A. E., & Loeb, A. 2005, MNRAS, 363, 353
Bromley, B., Melia, F., & Liu, S. 2001, ApJ, 555, L83
Dermer, C. D., Miller, J. A., & Li, H. 1996, ApJ, 456, 106
Eckart, A., et al. 2004, A&A, 427, 1
———. 2006, A&A, 450, 535
Eisenhauer, F., et al. 2005, ApJ, 628, 246
Fermi, E. 1949, Phys. Rev., 75, 1169
Genzel, R., et al. 2003, Nature, 425, 934
Ghez, A. M., et al. 2004, ApJ, 601, L159
———. 2005, ApJ, 635, 1087
Gillessen, S., et al. 2006, ApJ, 640, L163
Goldwurm, A., et al. 2003, ApJ, 584, 751
Hornstein, S., et al. 2002, ApJ, 577, L9
Liu, S., & Melia, F. 2002, ApJ, 566, L77
Liu, S., Melia, F., & Petrosian, V. 2006, ApJ, 636, 798
Liu, S., Petrosian, V., & Melia, F. 2004, ApJ, 611, L101
Mahadevan, R., Narayan, R., & Yi, I. 1996, ApJ, 465, 327
Markoff, S., Falcke, H., Yuan, F., & Biermann, P. L. 2001, A&A, 379, L13
Melia, F. 2006, The Galactic Supermassive Black Hole (Princeton: Princeton Univ. Press)
Melia, F., Liu, S., & Coker, R. 2000, ApJ, 545, L117
———. 2001, ApJ, 553, 146
Nayakshin, S., Cuadra, J., & Sunyaev, R. 2004, A&A, 413, 173
Park, B. T., & Petrosian, V. 1995, ApJ, 446, 699
Petrosian, V. 1981, ApJ, 251, 727
Petrosian, V., & Liu, S. 2004, ApJ, 610, 550
Porquet, D., et al. 2003, A&A, 407, L17
Schlickeiser, R. 1984, A&A, 136, 227
Schödel, R., et al. 2002, Nature, 419, 694
Tagger, M., & Melia, F. 2006, ApJ, 636, L33
Yuan, F., Quataert, E., & Narayan, R. 2003, ApJ, 598, 301
———. 2004, ApJ, 606, 894
Yusef-Zadeh, F., et al. 2006, ApJ, 644, 198
Zhao, J. H., Herrnstein, R. M., Bower, G. C., Goss, W. M., & Liu, S. M. 2004, ApJ, 603, L85